NASA TECHNICAL MEMORANDUM

NASA TM-78857

NASA TM-78857

NUMERICAL SPATIAL MARCHING TECHNIQUES FOR ESTIMATING DUCT ATTENUATION AND SOURCE PRESSURE PROFILES

by K. J. Baumeister
Lewis Research Center
Cleveland, Ohio 44135

TECHNICAL PAPER to be presented at the
Ninety-fifth Meeting of the Acoustical Society of America
Providence, Rhode Island, May 16-19, 1978

NUMERICAL SPATIAL MARCHING TECHNIQUES FOR ESTIMATING DUCT ATTENUATION AND SOURCE PRESSURE PROFILES

by K. J. Baumeister

NASA Lewis Research Center

Cleveland, Ohio 44135

ABSTRACT

A numerical method is developed that could predict the pressure distribution of a ducted source from far-field pressure inputs. Using an initial value formulation, the two-dimensional homogeneous Helmholtz wave equation (no steady flow) is solved using explicit marching techniques. The Von Neumann method is used to develop relationships which describe how sound frequency and grid spacing effect numerical stability. At the present time, stability considerations limit the approach to high frequency sound. Sample calculations for both hard and soft wall ducts compare favorably to known boundary value solutions. In addition, assuming that reflections in the duct are small, this initial value approach is successfully used to determine the attenuation of a straight soft wall duct. Compared to conventional finite difference or finite element boundary value approaches, the numerical marching technique is orders of magnitude shorter in computation time and required computer storage and can be easily employed in problems involving high frequency sound.

E-9586

INTRODUCTION

A detailed knowledge of a fan noise source is required in the design of turbojet engine acoustic suppressors, since the energy attenuation of the suppressor is strongly dependent on the radial and circumferential pressure distribution of the noise source (ref. 1). Recent experimental and analytical research (refs. 2 to 5) has focused on determining the radial and circumferential variations in acoustic pressure for typical turbofan sources from both internal and far-field pressure measurements.

The direct calculation of the internal structure of a ducted noise source from far-field pressure measurements is essentially an initial value problem.

If pressure and impedance are known at the boundary of the system (far-field), the pressure can be uniquely determined in the vicinity of the inlet as well as inside the inlet ducting which may contain acoustic energy absorbers in the wall. As an alternate to the statistical approach of Ref. 5, a relatively simple numerical marching method is developed by which this information, if available in the far-field, could be translated directly into a description of a ducted noise source.

In the absence of mean flow, explicit initial value numerical marching techniques are developed to obtain a solution to the homogeneous Helmholtz equation for a two-dimensional cartesian coordinate system. The technique uses the finite difference representation of the Helmholtz equation. Explicit marching schemes are emphasized since they reduce the solution of the Helmholtz equation to a simple algebraic algorithm which requires a minimum of computer storage and running time. Several sample calculations are also presented to illustrate how a source could be predicted from duct far-field conditions.

In addition, assuming that reflections in the duct are negligible, the technique is used to determine the attenuation of a straight two-dimensional soft wall duct by prescribing a pressure distribution and the acoustic impedance of the medium ($\rho_o^* c_o^*$) as the initial conditions at the source (see Symbols for all symbol meanings).

The truncation error and stability of these various marching schemes are studied. In particular, the Von Neumann method is used to develop relationships which describe how sound frequency, transverse grid spacing and marching step size affect numerical stability.

SYMBOLS

A_n Fourier coefficient, Eq. B1

a quadratic constant, Eq. 26

a_m difference coefficient

a_n Fourier coefficient, Eq. 18

b_m difference coefficient

c quadratic constant, Eq. 27

c_m	difference coefficient
c_o^*	speed of sound
d	parameter, Eq. 28
d_m	difference coefficient
ΔdB	sound attenuation
E_x	acoustic power
e_m	difference coefficient
f*	frequency
H*	channel height
I_x	acoustic-intensity in axial direction
i	$\sqrt{-1}$
J	total number of grid points in y direction
K	total number of grid points in x direction
L*	length of duct
m_s	spinning mode number
N	constant
n	transverse mode number
p	dimensionless Fourier coefficient of pressure p(x, y), p^*/p_A^*
p_A^*	amplitude of pressure fluctuation or $\rho_o^* c_o^{*2}$
p_m	pressure defined by Eq. 51
$\|p\|$	pressure amplitude, Eq. 10
$\|p\|_x$	averaged $\|p\|$, Eq. 11
$p_{k,i}$	discrete pressure at k_{ij} grid point
r	radial coordinate
u	dimensionless acoustic particle velocity in x direction $u^*\rho_o^*\omega^*H^*/p_A^*$
v	dimensionless acoustic particle velocity in y direction $v^*\rho_o^*\omega^*H^*/p_A^*$
W	weighting factor
x	dimensionless axial coordinate, x*/H*
x*	axial coordinate
Δx	axial grid spacing

y	dimensionless transverse coordinate, y^*/H^*
y^*	transverse coordinate
Δy	transverse grid spacing
z^*	acoustic impedance
ϵ	error in pressure
ξ	specific acoustic impedance
η	dimensionless frequency, f^*H^*/c_o^* or $\omega^*H^*/2\pi c_o^*$
θ	parameter, Eq. 29
λ^*	wavelength
ρ_o^*	density
φ	axial error variation parameter
ψ	angular coordinate
ω^*	circular frequency

Subscripts

e	exit condition
k	axial index, see Fig. 1
j	transverse index, see Fig. 1
m	cell index
n	harmonic component
o	entrance, x = 0
w	wall

Superscripts

*	dimensional quantity
$(\bar{\ })$	complex conjugate
(1)	real part
(2)	imaginary part

NUMERICAL APPROACH

Boundary Value Problem

The calculation of the propagation of sound in ducts using numerical finite difference and finite element techniques has been described in Refs. 6 to 12. Figure 1 shows a typical finite-difference grid network used in Ref. 6 to study

the propagation of sound in a two-dimensional duct. In this case, the derivatives in the propagation equations are expressed in terms of the values of pressure at each grid point. For the boundary conditions, an entrance pressure profile, wall impedance, and an exit impedance are required. The collection of the various difference equations at each grid point form a set of simultaneous equations which are solved to determine the pressure at each grid point. A similar procedure is used in the finite element theory. In general, the finite element technique is more convenient to use for complex geometries (ref. 9), although it requires larger solution times than the finite difference techniques.

The grid system does not have to be confined to the region inside the duct, as shown in Fig. 1, but it may also be extended to regions external to the duct, as depicted in Fig. 2(a). Grid points may be extended into the far-field by a direct placement of grid nodes or elements in the far-field, such as used in Ref. 12 for a flanged horn or by some type of mapping function (Ref. 7).

However, the boundary value approach presents some severe difficulties. Generally, numerical solutions to the boundary value acoustic problems are limited to relatively low frequency sound and relatively short ducts, because at least 12 axial grid points or elements are required per wavelength of sound in order to accurately estimate the acoustic intensity (Ref. 6). A wave envelope analysis was developed in Refs. 8 and 10 to overcome this difficulty; however, the technique has only been applied to the simple cases of no flow and plug flow.

Initial Value Problem

In an initial value problem both the pressure and impedance either in the far-field or at the noise source are known. This is illustrated in Figs. 2(b) and (c). Using a marching technique, the pressure at the points adjacent to the boundary can be immediately calculated. The matrix algebra and computer storage associated with the boundary value problem is unnecessary for the initial value problem. Since no matrix of coefficients has to be stored and manipulated as in the boundary value problem, marching techniques are not limited to low frequency problems. However, associated with marching techniques is the prob-

lem of numerical stability; that is, preventing the growth of the round-off errors.

Next, the governing equation will be presented along with the formulation of the initial value approach.

ANALYTIC MODEL

Governing Equations and Boundary Conditions

For a two dimensional duct with no flow, assuming that the pressure is a simple harmonic function of time ($e^{i\omega t}$) and that no sources exist in the medium, the linearized gas-dynamic equations (Ref. 13, p. 5) of continuity, momentum, and energy reduce to the dimensionless Helmholtz equation

$$\frac{\partial^2 p}{\partial x^2} + \frac{\partial^2 p}{\partial y^2} + (2\pi\eta)^2 p = 0 \tag{1}$$

The acoustic velocities are given as (Ref. 10)

$$u = i \frac{\partial p}{\partial x} \tag{2}$$

$$v = i \frac{\partial p}{\partial y} \tag{3}$$

(The dimensional quantities used to normalize the above parameters are given in the Symbols section.) In these coordinates, the following boundary conditions apply at the upper wall

$$\zeta_w = \frac{z_w^*}{\rho_o^* c_o^*} = \frac{1}{\rho_o^* c_o^*} \frac{p^*}{v^*} = \frac{-i 2\pi\eta p}{\left.\frac{\partial p}{\partial y}\right|_w} \tag{4}$$

or

$$\left.\frac{\partial p}{\partial y}\right|_w = \frac{-i 2\pi\eta p_w}{\zeta_w} \tag{5}$$

where ζ_w is the complex specific acoustic wall impedance. At the lower wall ($y = 0$) the signs are changed. The starred quanties indicate dimensional terms while the unstarred terms are dimensionless. Similarily (Ref. 10, Eq. 35) the axial impedance condition is

$$u_e = i \left.\frac{\partial p}{\partial x}\right|_e = \frac{2\pi\eta}{\zeta_e} p_e \tag{6}$$

The sound power that leaves a duct and reaches the far-field is related to the instantaneous axial intensity at the duct exit. The intensity can be expressed in dimensionless form as

$$I_x = \frac{1}{2\pi\eta} \text{Real}(p\bar{u}) \tag{7}$$

where the bar denotes the complex conjugate. The total dimensionless acoustic power is the integral of the intensity over the transverse dimension y

$$E_x = \int_0^1 I_x(x, y)\, dy \tag{8}$$

By definition, the sound attenuation (decrease in decibels of the acoustic power from x = 0 to x) can be written as

$$\Delta dB = 10 \log_{10} \frac{E_x}{E_o} \tag{9}$$

The pressure amplitude |p| is a quantity to indicate how the acoustic pressure varies in the duct. By definition

$$|p| = \sqrt{p\bar{p}} = \sqrt{p^{(1)2} + p^{(2)2}} \tag{10}$$

where $p^{(1)}$ and $p^{(2)}$ are the real and imaginary parts of p respectively. A useful quantity in comparing the boundary value and marching solution is

$$|p|_x = \int_0^1 \sqrt{p\bar{p}}\, dy \tag{11}$$

which gives a measure of the pressures across the entire transverse dimension of the duct.

Finite Difference Formulation

Instead of a continuous analytical solution for pressure, marching solutions determine the pressure at isolated grid points by means of finite-difference approximations. The differential governing equation, in this case Eq. 1, will be expressed as an algebraic equation in terms of the pressures at the grid points. In the initial value problem to be considered here, the pressures at the grid

points adjacent to the known boundary are found from the known pressure and impedance at the boundary.

The governing difference equation can be developed by an integration process in which the Helmholtz Eq. 1 is integrated over the various cell areas shown in Fig. 3

$$\int_{\text{Cell area}} \left(\frac{\partial^2 p}{\partial x^2} + \frac{\partial^2 p}{\partial y^2} + (2\pi\eta)^2 p \right) dy dy = 0 \tag{12}$$

The finite-difference approximations for the various cells shown in Fig. 3 are expressed in terms of the coefficients

$$a_m p_{k-1,j} + b_m p_{k,j-1} + c_m p_{k,j} + d_m p_{k,j+1} + e_m p_{k+1,j} = 0 \tag{13}$$

The subcript m denotes the cell number. The expressions for the coefficients for the various cells can be found in Table I. The derivation of cell 1 of Table I is presented in Appendix A of this paper. The derivation of the coefficients for the other cells can be found in Ref. 10 (Appendix D) and will not be presented here.

The explicit marching technique is based on the face that $p_{k-1,j}$ is the only unknown. Therefore, the pressure at (k-1, j) can be solved directly as

$$p_{k-1,j} = -\frac{1}{a_m} (b_m p_{k,j-1} + c_m p_{k,j} + d_m p_{k,j+1} + e_m p_{k+1,j}) \tag{14}$$

The above equation can be used in marching backward from the end of the duct as shown in Fig. 3(a). On the other hand, if we start from x equal 0 at the duct inlet and move towards the duct exit, then $p_{k+1,j}$ would become the unknown. In this case, the marching could be started with cell Eqs. 7, 8, and 9 of Fig. 3(b).

STABILITY CONSIDERATIONS

Stability Problem

Equation 14 was applied to the problem of a hard wall duct with a plane wave existing at the exit ($L^*/H^* = 1$) and an exit impedance equal to $\rho_o^* c_o^* (\zeta_e = 1)$. A solution for $|p|_x$ defined by Eq. 11 is displayed in Fig. 4 for a frequency

parameter of $\eta = 1$. The known analytical solution is given in Ref. 8 for a plane wave in a hard wall duct

$$p = \cos 2\pi\eta x - i \sin 2\pi\eta x \tag{15}$$

or substituting into Eqs. 10 and 11 yields

$$|p|_x = 1 \tag{16}$$

As seen in Fig. 4, the numerical values of $|p|_x$ are in close agreement with the analytical value until the axial position, x equals 0.4, is reached. Obviously, an instability occurs as the solution is marched from the exit (x = 1.0) to the entrance (x = 0). Clearly, the explicit marching equation as given by Eq. 14 is unstable in this case. Consequently, a detailed analysis of the stability of the Hemholtz equation is required, to determine when instabilities can occur and how they can be avoided.

Von Neumann Method

To analyze the stability of the difference approximation to the Helmholtz equation, we must study how the errors introduced into the computation propagate. We may express the exact solution to the difference equation in the form

$$p(\text{exact}) = p(\text{computed}) + \epsilon(\text{error}) \tag{17}$$

The error may be due to round-off or a computational mistake. The propagation of errors through the computation is governed by the original difference equation. Assuming the initial and boundary values for the error are zero, then the equation governing the propagation of errors is the homogeneous form of the defining difference equation, Eq. 13.

For difference relations involving constant coefficients, the errors may be expanded in a finite Fourier series of the form

$$\epsilon_{k,j} = \sum_n a_n \varphi^k(n)\, e^{in\pi y_j} \tag{18}$$

This expression for the error was first used by Von Neumann (Ref. 14 and 15). The problem of stability is studied by noting the behavior of the coefficients $\varphi(n)$. If any $\varphi(n)$ is such that

$$|\varphi(n)| > 1 \tag{19}$$

for any n, then the corresponding error harmonic would grow beyond limit during during marching.

Stability Analysis

The stability analysis will be performed for the two marching schemes shown in Fig. 5. In these cases, the (k+1, j) values are considered the unknown, in contrast to the earlier examples where we were moving from the exit to the entrance of a duct. The explicit schemes shown in Fig. 5 allow the pressures to be calculated from a simple algebraic equation of the form of Eq. 13.

To cover these two grid patterns, the stability analysis will be developed for the grid network shown in Fig. 5(b). In this network, the difference approximation for the Helmholtz wave equation (see Appendix A) becomes

$$\begin{aligned} p_{k+1,j} - 2\,p_{k,j} + p_{k+1,j} = &- W_k \left(\frac{\Delta x}{\Delta y}\right)^2 (p_{k,j+1} - 2\,p_{k,j} + p_{k,j-1}) \\ &- W_{k-1} \left(\frac{\Delta x}{\Delta y}\right)^2 (p_{k-1,j+1} - 2\,p_{k-1,j} + p_{k-1,j-1}) \\ &- (2\pi\eta\Delta x)^2\, p_{k,j} \end{aligned} \tag{20}$$

where

$$W_k + W_{k-1} = 1 \tag{21}$$

The weighting factors W_k and W_{k-1} indicate the importance of a particular grid approximation in the model. For example, if W_{k-1} equals zero, then Eq. 20 would represent the Explicit x grid of Fig. 5(a).

Since the propagation errors are also governed by Eq. 20, Eq. 18 (for a particular n) is substituted into Eq. 20 with $\epsilon_{k,j}$ replacing $p_{k,j}$. Dividing through the resulting equation by $a_n \varphi^k e^{in\pi y_j}$, regrouping terms with the like values of φ^k and noting that

$$e^{iny_{j+1}} \Big/ e^{iny_j} = e^{in\Delta y} \tag{22}$$

$$e^{iny_{j-1}} \Big/ e^{iny_j} = e^{-in\Delta y} \tag{23}$$

and

$$e^{in\pi\Delta y} - 2 + e^{-in\pi\Delta y} = -2(1 - \cos n\pi\Delta y, = -4 \sin^2 \frac{n\pi\Delta y}{2} \tag{24}$$

then the solution for φ obeys the quadratic form

$$a\varphi^2 - 2\varphi + c = 0 \tag{25}$$

where

$$a = \left| \frac{1}{1 + \theta W_k/2 - d/2} \right| \tag{26}$$

$$c = \left| \frac{1 - \theta W_{k-1}}{1 + \theta W_k/2 - d/2} \right| \tag{27}$$

$$d = (2\pi\eta\Delta x)^2 \tag{28}$$

$$\theta = 4 \left(\frac{\Delta x}{\Delta y}\right)^2 \sin^2 \frac{n\pi\Delta y}{2} \tag{29}$$

The well known solution for φ is written as

$$\varphi = \frac{1}{a} \pm \sqrt{\frac{1}{a^2} - \frac{c}{a}} \tag{30}$$

So that the errors will not grow, $|\varphi|$ must have a value less than unity (see Eq. 19). This requires that the coefficients a and c obey the following inequalities

$$-1 < \frac{1}{a} < 1 \tag{31}$$

and

$$-1 + \frac{2}{|a|} < c/a < 1 \tag{32}$$

However, it is convenient to use a more restricted form of Eq. 31

$$0 < \frac{1}{a} < 1 \tag{33}$$

Eqs. 32 and 33 put stability restrictions on the maximum allowable size of axial spacing Δx; however, Δx must be restricted to even smaller values to reduce truncation error. From Ref. 6, the required number of axial grid points was

$$K = N\eta\, L^*/H^* \qquad N \geq 12 \tag{34}$$

Thus,

$$\Delta x = \frac{L^*/H^*}{K} < \frac{1}{12\eta} \tag{35}$$

Also, the transverse spacing Δy was given in Ref. 6 by

$$\Delta y = \frac{1}{J-1} \tag{36}$$

However, no requirement for the size of transverse spacing Δy was given in Ref. 6 other than the number of transverse grid points be increased until convergence is achieved.

Finally, whenever Eqs. 32 and 33 are conservatively applied, the sine term in Eq. 29 is assumed to take on the maximum possible value

$$\sin^2 \frac{n\pi\Delta y}{2} = 1 \tag{37}$$

Now, Eqs. 32 to 37 will be applied to the grid forms in Fig. 5.

Explicit X-grid. - For the simplest explicit X-grid (Fig. 5(a)), the weighting factor W_{k-1} is zero and W_k equals 1. Thus

$$a = \left[1 + (\theta/2) - (d/2)\right]^{-1} \tag{38}$$

and

$$c/a = 1 \tag{39}$$

Applying the first condition for stability, Eq. 33, yields $d > \theta$ where θ and d are defined by Eqs. 28 and 29 respectively.

Hence,

$$\Delta y > \frac{1}{\pi\eta} \left| \sin \frac{\pi\eta\Delta y}{2} \right| \tag{40}$$

Finally using Eq. 37 yields the following requirement for numerical stability of the 5 point X-grid shown in Fig. 5(a)

$$\Delta y > \frac{0.32}{\eta} \quad \Delta y^* > \frac{0.32}{f^*/c_o^*} = 0.32\,\lambda^* \tag{41}$$

Along with Eq. 41, the second condition for stability, Eq 32, must also hold, but the right hand side of Eq. 32 can not be satisfied since c/a in Eq. 39 is identical to 1. In this case, the solution for φ occurs as complex pairs of magnitude equal to unity

$$\varphi = 1, \text{ if } \Delta y > \frac{0.32}{\eta} \text{ and } \Delta x < \frac{1}{12\eta} \tag{42}$$

Such a case is defined (Ref. 14, p. 337) as having a linear instability.

At first glance, these results, Eqs. 41 and 42, are disappointing. Consider Eq. 41. With numerical techniques it is desirable to have Δx and Δy related so that both Δx and Δy can both be decreased to zero to check convergence. However, in this special case of the Helmholtz equation, this limitation on Δy has an important physical interpretation. Also, Eq. 42 has the exact property ($\varphi = 1$) required for acoustic calculations. Both Eqs. 41 and 42 will now be considered, beginning first with Eq. 42.

The Fourier components for propagating transverse acoustic modes should travel with undiminished amplitudes in hard wall ducts (see Eq. B1 - Appendix B or Ref. 16). Since φ could represent the x dependence of a pressure wave just as well as an error, φ must be held at one in the numerical calculation. Thus, Eq. 42 has exactly the properties desired in modeling acoustic propagation down a hard wall duct for propagating transverse modes. That is, the amplitude of the waves in the x direction is constant ($\varphi = 1$). Other nodal systems could be used in this problem besides the two shown in Fig. 5. However, if φ should

be significantly different from one, this method would lead to incorrect answers.

Unfortunately, if φ equals one, errors are also not diminished in magnitude either. Errors at successive steps may accumulate and because of linear instability the amount of round-off error may ultimately become the dominant factor in the calculation if many grid points are used (Ref. 15).

Explicit H-grid. - To prevent the accumulation of errors, the 7 point or explicit H-grid will be employed, as shown in Fig. 5(b). In this case, the weighting factor W_{k-1} is kept at a small value (10^{-6}) so that φ will be slightly less than one so, that errors do not grow. However, because W_{k-1} is such a small value, φ can be considered equal to one for practical purposes. Consequently, the decrease in amplitude of the desired propagating transverse mode will be negligible.

To first order, the stability criteria for Δx and Δy are the same as for the 5-point or explicit X-grid shown in Fig. 5(a). The explicit X-grid will, however, still be used to start the marching solution. In such a case, the error associated with a single step would be negligible.

Now, let us return to Eq. 41 for a physical interpretation of its meaning. Assume that the argument of the sine term in Eq. 40 is small such that

$$\sin \frac{\pi n \Delta y}{2} \sim \frac{\pi n \Delta y}{2} \tag{43}$$

Substituting Eq. 43 into Eq. 40 yields

$$n < 2\eta \tag{44}$$

Eq. 44 represents the cutoff condition for a mode to propagate unattenuated down a hard wall rectangular duct (see Eq. B2, Appendix B). Therefore, Eqs. 41 and 42 can be interpreted to mean that only propagating modes can be handled in the calculation.

Using Eq. 36 with Eq. 41, the increment Δy can be expressed in terms of the number of grid points J in the y direction as

$$J < \pi\eta + 1 \tag{45}$$

For a given harmonic to exist in the solution, there must be sufficient grid points

to resolve a Fourier component. To define a wave, at least 2 points are required. Therefore

$$n \gtrsim \frac{J}{2} \tag{46}$$

or substituting Eq. 46 into Eq. 45 yields

$$n < \frac{\pi\eta + 1}{2} \tag{47}$$

which is roughly equivalent to Eq. 44 for small values of η. Thus, the stability criteria indicate that marching could be unstable if sufficient grid points are available to resolve the higher order transverse modes.

As will be shown later, the restriction of handling only propagating modes will limit the useful application of this technique to high frequency (high η) calculations and to those problems where the cut-off modes do not play an important part in matching pressure or other boundary conditions.

DIFFERENCE ALGORITHM

The marching equation for calculating pressure down the duct for the central cell can now be written from Eq. 20 as

$$p_{k+1,j} = (2 - (2\pi\eta\Delta x)^2)\ p_{k,j} - p_{k-1,j} + W_k\left(\frac{\Delta x}{\Delta y}\right)^2 (-p_{k,j+1} + 2\,p_{k,j} - p_{k,j-1})$$

$$+ W_{k-1}\left(\frac{\Delta x}{\Delta y}\right)^2 (-p_{k-1,j+1} + 2\,p_{k-1,j} - p_{k-1,j-1}) \tag{48}$$

For the upper wall cell, soft wall boundary conditions require that

$$p_{k+1,j} = (2 - (2\pi\eta\Delta x)^2)\ p_{k,j} - p_{k-1,j} + 2\,W_k\left(\frac{\Delta x}{\Delta y}\right)^2 \frac{i2\pi\eta\Delta y}{\xi_k}\, p_{k,j} + p_{k,j} - p_{k,j-1}$$

$$+ 2\,W_{k-1}\left(\frac{\Delta x}{\Delta y}\right)^2 \frac{i2\pi\eta\Delta y}{\xi_{k-1}}\, p_{k-1,j} + p_{k-1,j} - p_{k-1,j-1} \tag{49}$$

The equation at the lower wall requires that j - 1 in Eq. 49 becomes j + 1. For W_{k-1} equal to 10^{-6}, the equations represent the explicit H-grid system. For W_{k-1} equal zero and W_k equal unity, the equations represent the explicit X-grid.

DUCT MARCHING EXAMPLES

To illustrate the capabilities and limitations of the marching technique, sample problems will be presented for the simplest case of a two-dimensional duct as shown in Fig. 6, instead of the more complicated geomtry shown in Fig. 2. The advantage of this simplification is that a direct comparison of numerical and analytical techniques can be made. A boundary value solution for Fig. 6(a) can be used to set up the exact exit conditions for the problems in Figs. 6(b) and (c). As a result, the numerical accuracy of the marching technique can be conveniently checked for the case of soft wall ducts.

Hard Wall Ducts

In the example shown in Fig. 7, the stability condition for a hard wall duct is evaluated for decreasing values of Δy (increasing J) for various modal inputs at a dimensionless frequency η equals 3. As seen in Fig. 7, for the first mode (n = 0), the calculations are convergent to the analytical solution for J considerably larger than the value of 10 predicted by Eq. 45. It is likely that the round off error is quite small for a plane wave and the calculation is terminated before the error can grow to a significant value. On the other hand, the higher order transverse modes (n > 0) follow the stability criteria quite closely.

As an additional check shown in Fig. 8, the number of grid points in the x direction was increased to test for stability. As theory predicted, the results remain converged.

Soft Wall Duct

Next, the marching technique is applied to a soft wall duct. From Ref. 10, the boundary value finite difference solution for a plane wave input was used to establish the exit conditions. The results are shown in Fig. 9. As can be seen in Fig. 9, the explicit H-grid marching technique and the boundary value technique

are in exact agreement. Again there was no error growth when the number of axial grid points was increased.

Phase Relationship

A marching theory was devised so that the acoustic pressure distribution at a source might be deduced from far-field measurements. In actual practice, Refs. 17 and 18 for example, sound pressure level measurements are recorded at a set of microphone stations in the far-field without regard to the phase relationship between the various microphone measurements. In the next example, the sensitivity of the duct attenuation and source profiles to a change in phase at the duct exit is considered.

For the same problem considered in Fig. 9, again the finite difference solution from Ref. 10 was used to establish the exit condition. The solid line shown in Figs 10 and 11 indicates results based on the correct phase relationship as computed from the boundary value analysis. On the other hand, the dotted line in Figs. 10 and 11 presents a calculation with an exit pressure of the same absolute pressure magnitude (SPL) but of different phase. In this case, the imaginary part of the acoustic pressure $p^{(2)}$ was assumed to be zero. As seen in Fig. 10, the improper phase relationship leads to much higher attenuations. Fig. 11 shows a pronounced effect of the exit phase on the calculated source pressure profile. Obviously a considerably different pressure profile from that of a plane wave has been generated at the liner entrance. Clearly, if one wishes to establish the structure of the noise source from far-field measurements, the far-field measurement must include a reference microphone to establish the phase.

FAR-FIELD APPLICATION

As mentioned in the introduction, the impetus to develop the marching tech technique came from a desire to establish the noise source from far-field data. The purpose of this section is to discuss the possible application of this technique in obtaining information on the spinning mode content of a turbofan engine.

In analyzing far-field data from a typical turbofan engine, cylindrical and

spherical type coordinate systems should be used to resolve the fan's radial, circumferential (inside duct) and axial pressure. In such a case, a three dimensional differential wave equation of the form (inside duct)

$$L\left\{p(r, \psi, x)\right\} = 0 \tag{50}$$

is required. The differential operator L should, of course, be sufficiently general to account for variable mean flow Mach numbers and variable inlet geometry. The operator could be cylindrical coordinates inside the duct and spherical coordinates outside the duct. The coordinate system would be coupled at the duct exit using some type of matching (see Ref. 19).

Inside the duct, the circumferential variable ψ could be separated by assuming a pressure distribution of the form

$$p(r, \psi, x) = p_m(r, x)\, e^{im_s\psi} \tag{51}$$

where m_s is the "spinning" mode number. Therefore, the equation describing the pressure field reduces to a simplier two-dimensional form,

$$L\left\{p_m(r, x)\right\} = 0 \tag{52}$$

Now, let us consider the possible application of Eq. 52 to a numerical solution for the noise source based on far-field data.

To estimate the modal content of a fan source using the marching technique, a matrix of grid points would be placed in the acoustic field leading from the microphones to the fan source. Assume that the microphones are spaced about a fan inlet at some fixed height above the ground under free field conditions. Furthermore, assume the microphones are set to measure both magnitude and phase of the pressure. As was shown in the last example of the previous section, phase information is necessary to account for cancellation of the various modes in the duct and the far-field.

Unfortunately, a unique solution exists at the fan source for any assumed mode number m_s; that is, a lobe pattern in the far-field would transfer (by marching) to a radial shape in the duct at the source. For numerical calculations,

the range of m_s would be limited to low values of m_s (Ref. 3) so that some propagating radial modes exist in the duct. For large values of m_s, most if not all of the radial modes no longer propagate as a wave (Ref. 16, p. 497). Although analytical solutions might allow predictions of the noise source for large m_s, such a solution would be no practical interest since the pressure would propagate by diffusion (like heat) and errors in measurement would be highly magnified (Ref. 20, pp. 229-231). The Von Neumann analysis will again limit the grid spacing to allow only propagating modes in the duct.

Although only propagating modes exist in a duct near its exit, higher order far-field modes can be generated at the exit by a change of geometry (Ref. 21, p. 122 or Ref. 22), in this case the inlet lip of a turbofan engine. Therefore, since all modes propagate in the far-field (Ref. 13, p. 212), in applying the marching technique to the far-field, the grid structure must account for a full range of acoustic modes. This will be the case since the number of grid points can increase because of the inlarged area available in the far-field. That is, using a rectangular system for example, Δy is constant both inside and outside the duct, Eq. 42; consequently, more grid points can be used in the far-field.

Because the spinning mode number m_s is not known, and the source will be multimodal, measurements from a far-field horizontal array of microphones alone can not uniquely determine the circumferential modal content of a fan. In effect, a horizontal traverse in the far-field is analogous to a radial traverse internal to the duct, neither of which give any information on the circumferential modal content of the source. This agrees with the theory of Ref. 5.

If the marching method is to be used to deduce circumferential modal patterns inside the duct without using any apriori assumptions about the modal content, additional pressure measurements must be taken in the far-field in the colatitude direction (Ref. 23, p. 60). A three dimensional solution of the complete set of far-field data would lead to a source distribution $p(r, \psi, 0)$ at the fan face. This would be decomposed (Fourier series) into the various circumferential modes.

If the phasing among the modes is a random variable such as for broadband

noise or if a large number of modes are involved even for a discrete tone, the direct solution for duct modes from far-field measurements might not be practical. For these cases an approximate approach such as used in Ref. 3 or 4 might be used.

SUPPRESSOR ATTENUATION WITH PLANE WAVE INPUT

The noise attenuation of a suppressor is now evaluated using the marching techniques. Consider the attenuation produced in the beginning length L^* of an infinitely long duct which has a uniform impedance along its entire length, as shown in Fig. 12(a). To numerically predict the attenuation of the entrance length L^* in the infinite duct (Ref. 6 to 10), a finite duct of length L^* (Fig. 12(b)) is used with an assumed exit impedance hopefully equal to the impedance which exists at L^* in the infinite duct.

An infinitely long duct with uniform impedance will not have any reflections at any position in the duct. Consequently, the wave propagation in the entrance region of the infinite duct can be represented with a numerical solution to a finite duct of length L^*, as in Fig. 12(b), by choosing the exit impedance at L^* so that the reflections are minimized. For the case of zero mean flow, and a plane wave input, a $\rho_0^* c_0^*$ exit impedance was found to give good agreement between the analytical and numerical results for η between 1 and 5 and L^*/H^* between 0.5 and 6 (Ref. 8, Fig. 9).

Herein, the axial impedance of the medium is assumed to be constant down the duct; consequently, the impedance of the medium at the noise source ($x = 0$) is also assumed to be $\rho_0^* c_0^*$. This entrance impedance assumption precludes any possibility of reflections at the duct entrance and would not be valid in cases where strong reflections are known to exist. Using this assumption and the marching technique, the noise attenuation at the optimum point (point of maximum attenuation in the impedance plane) is now calculated for a two-dimensional duct with L^*/H^* values ranging between 0.5 and 5 and an input plane wave with dimensionless frequencies η of 1, 2, and 5. The values of the optimum liner impedance used in the numerical analysis were determined from the analytical

techniques presented in Ref. 24.

The numerically calculated attenuations are compared to the corresponding analytical results in Fig. 13. The numerical results are given by symbols while the analytical results are represented by the solid lines. For dimensionless frequencies η equal to 1 or 2, the numerical and analytical results are generally in poor agreement. Also, for η equal to 1, the analysis breaks down (calculated numbers go to infinity) for L^*/H^* equal or greater than one, while for η^* equal to 2 the break down begins at L^*/H^* equal to 3. Most likely, the truncation error is large because there are few points in the transverse y direction. In the case of η equals 1, Eq. 45 allows the use of only 4 points.

On the other hand, the analytical and numerical results are in very good agreement for η equal to 5. It is well known (Ref. 25, p. 391), that the truncation error is dominated by the largest spacing increment, in this case Δy. For high frequencies, sufficient transverse grid points are now available to reduce the truncation error in the y-direction and thereby to accurately predict the transverse pressure profiles. Therefore, stability restrictions on Δy limit the application of the marching technique to high frequency sound, η equal to 5 or greater. This limitation applies equally well to the work of the previous section (marching from the duct exit to the entrance).

In the simple but practical example just considered, reflections in the duct do not exist. In such a case, the aerodynamic forces producing the noise source could be calculated without reference to the acoustic field. However, a wide class of problems exists in which the acoustic field reacts back in the source (Ref. 26), such as when partial blockage (scattering) occurs in a duct (Ref. 16, p. 400) or when a duct mode produces a large back reaction force on the source (Ref. 16, p. 501). In these more complicated situations, an iterative marching approach might account for reflections in the system.

CONCLUDING REMARKS

1. An initial value numerical method is developed to predict the pressure distribution of a ducted source from the downstream pressure measurements. The technique is useful for relatively high frequencies ($\eta \geq 5$). For the special case where reflection in a duct are small; the technique can also be used to estimate the attenuation of a straight soft wall duct.

2. Compared to conventional finite difference or finite element boundary value approaches, the numerical marching technique is orders of magnitude shorter in computational time and computer storage requirements. Therefore, this technique could be used as a companion to the boundary value techniques particularly at high frequencies.

3. The Von Neumann method accurately predicts the onset of instability in the numerical calculation. The stability considerations limit the approach to high frequency sound.

4. Because the marching technique is explicit in nature, the technique can readily be applied to three dimensional problem. Thus, the technique could be useful in tracing far-field pressure patterns back to the noise source. Example problems also indicate that the phase relationships between microphone measurements in the far-field must be recorded if the source distribution is to be calculated.

5. The marching technique, in effect, reduces the partial difference equation to an ordinary differential equation because the transverse gradient terms are approximated by previously known values. Thus, in principle, a nonlinear problem could be conveniently handled with Runga Kutta or other standard techniques. In addition, the techniques may be applicable to other complications in the flow field, such as a variable speed of sound (Ref. 27). Of course, the procedure would have to be first applied before one could be certain of its success. In these more complicated cases, the stability analysis could be performed by computer trial and error to determine critical values of Δy and Δx.

6. The marching technique can easily be applied directly to the individual continuity, momentum, and energy equations. Thus, it is unnecessary to combine these equations to obtain a wave equation. The combination was performed herein to simplify the stability analysis. Hopefully, with the addition of flow gradients and some nonlinear effects, the stability requirements will not be as restrictive.

7. Finally, the marching technique can not be used directly to estimate the attenuation of noise suppressors in situations where large reflections occur in a duct such as would occur with a converging duct. In this case, an assumed entrance impedance of $\rho_o^* c_o^*$ could be invalid. However, an iteration process might be developed which could lead to a valid solution. This limitation does not apply to situations where both the pressure and entrance impedance are known from measurements.

APPENDIX A

FINITE DIFFERENCE FORMULATION

The governing difference equation can be developed by an integration process in which the Helmholtz Eq. 1 is integrated over the cell area, Eq. 12. Eq. 12 can be rewritten as

$$\underset{\text{Cell area}}{\int\int} \frac{\partial^2 p}{\partial x^2}\,dxdy + \underset{\text{Cell area}}{\int\int} \frac{\partial^2 p}{\partial y^2}\,dxdy + \underset{\text{Cell area}}{\int\int} (2\pi\eta)^2\, p\,dxdy = 0 \qquad \text{(A1)}$$

The various pressures and their derivatives in Eq. A1 are evaluated at the edges of the cells, designated by + and - signs in the following equations. These terms will be different for each cell because the boundary conditions, as well as size of the cell vary.

For cell number 1 in Fig. 3, the standard approximations for the derivatives are used

$$\int\int \frac{\partial^2 p}{\partial x^2}\,dxdy = \left.\frac{\partial p}{\partial x}\right|_-^+ \int_-^+ dy = (p_{k+1,j} - 2\,p_{k,j} + p_{k-1,j})\,\frac{\Delta y}{\Delta x} \qquad \text{(A2)}$$

$$\int\int \frac{\partial^2 p}{\partial y^2}\,dxdy = \left.\frac{\partial p}{\partial y}\right|_-^+ \int_-^+ dx = (p_{k,j+1} - 2\,p_{k,j} + p_{k,j-1})\,\frac{\Delta x}{\Delta y} \qquad \text{(A3)}$$

$$\int\int (2\pi\eta)^2\, p\,dxdy = (2\pi\eta)^2\, p_{k,j} \int\int dxdy = (2\pi\eta)^2\, \Delta x \Delta y\, p_{k,j} \qquad \text{(A4)}$$

where

$$\left.\frac{\partial p}{\partial x}\right|^+ = \frac{p_{k+1,j} - p_{k,j}}{\Delta x}\,;\quad \left.\frac{\partial p}{\partial x}\right|_- = \frac{p_{k,j} - p_{k-1,j}}{\Delta x} \qquad \text{(A5)}$$

$$\left.\frac{\partial p}{\partial y}\right|_{+} = \frac{p_{k,j+1} - p_{k,j}}{\Delta y}\,;\quad \left.\frac{\partial p}{\partial y}\right|_{-} = \frac{p_{k,j} - p_{k,j-1}}{\Delta y} \tag{A6}$$

Substituting Eqs. A2 to A5 into Eq. A1 gives

$$-\left(\frac{\Delta y}{\Delta x}\right)^2 p_{k-1,j} - p_{k,j-1} + 2\left[1 + \left(\frac{\Delta y}{\Delta x}\right)^2 - \frac{(2\pi\eta\Delta y)^2}{2}\right] p_{k,j} - p_{k,j+1} - \left(\frac{\Delta y}{\Delta x}\right)^2 p_{k+1,j} = 0 \tag{A7}$$

The finite-difference approximation for cell no. 1, Eq. A7, as well as the other cells in Fig. 3 can be written in the form of Eq. 13 in the body of this report.

The derivation of the difference equations at the upper boundary are just as easy provided one recognizes that

$$\left.\frac{\partial p}{\partial y}\right|_{+} = \frac{-i2\,\eta\, p_{k,j}}{\zeta_w} \tag{A8}$$

as given by Eq. 5. Similar expression can be developed for the exit condition.

For the special case of the explicit H-grid shown in Fig. 5(b), the transverse grid derivatives at the upper wall would be approximated by

$$\left.\frac{\partial p}{\partial y}\right|_{-} = \frac{W_k(p_{k,j} - p_{k,j-1})}{\Delta y} + \frac{W_{k-1}(p_{k-1,j} - p_{k-1,j-1})}{\Delta y} \tag{A9}$$

$$\left.\frac{\partial p}{\partial y}\right|_{+} = \frac{-W_k\, i2\,\eta\, p_{k,j}}{\zeta_k\big|_w} - \frac{W_{k-1}\, i2\,\eta\, p_{k-1,j}}{\zeta_{k-1}\big|_w} \tag{A10}$$

The weighting factors W_k and W_{k-1} are defined by Eq. 21 in the body of this paper.

APPENDIX B

PHYSICAL SIGNIFICANCE OF VON NEUMANN METHOD

The Von Neumann method is quite compatible with acoustic problems since the Fourier representation of the error at each grid point can be also applied to an actual transverse harmonic pressure input at the boundary. Therefore, in addition to evaluating the stability of the various grid systems, let us consider what effects the governing equations and boundary conditions will have on a transverse harmonic input for the simple case of a hard wall duct.

The solution to the Helmholtz equation, Eq. 1, for a two-dimensional infinitely long duct with rigid walls is given for example in Ref. 16 (pp. 496 and 504). The nondimensional acoustic pressure can be expressed (using notation different from Ref. 16) as

$$p = \sum_{n=1}^{\infty} A_n \cos n\pi y \, e^{-i\pi \sqrt{(2\eta)^2 - n^2}\, x} \qquad \text{(B1)}$$

where the rigid walls are located at y equals 0 and 1. The symbol n represents the transverse mode number. The characteristic function $\cos n\pi y$ satisfies the condition that the transverse velocity at both walls will be identical to zero for a hard wall two-dimensional duct.

Eq. B1 indicates that for the mode number n, if

$$n < 2\eta \qquad \text{(B2)}$$

the mode ($\cos n\pi y$) will propagate unattenuated down the duct with a constant amplitude. On the other hand, if n is greater than 2η the mode will exponentially decay. It is said to be cutoff. For the special case of n equals 2η the mode becomes a transverse standing wave in the duct; that is, no variation exists in the x direction.

In a hard wall duct, if Eq. B2 is satisfied, the numerical marching technique should predict that the amplitude of a transverse harmonic wave will remain constant along the duct. This is precisely what occurs when Eq. 42 is satisfied;

that is, φ must be equal to one in the Von Neumann analysis. If φ were less than one, the transverse harmonic mode would decay with distance, which would violate the true physical situation as indicated by Eq. B1 for propating transverse pressure modes. Thus, the numerical marching technique has the proper characteristics to match the physical situation only if φ equals 1 in the Von Neumann analysis.

In the sample problems investigated in the body of this paper, plane wave and single transverse mode inputs were considered. For a plane wave input, Ref. 6 had found that an exit impedance of $\rho_o^* c_o^*$ is a good choice for both hard and soft wall ducts. However, for a single harmonic mode, the exit impedance associated with Eq. B1 is used. Substituting Eq. B1 into Eq. 2 yield for the axial acoustic velocity of the nth mode.

$$u_n = 2\pi\eta \sqrt{1 - \left(\frac{n}{2\eta}\right)^2}\, p_n \tag{B3}$$

Finally, substituting Eqs. B1 and B3 into Eq. 6 yields for the exit impedance

$$r_{n|e} = \left[1 - \left(\frac{n}{2\eta}\right)^2\right]^{-1/2} \tag{B4}$$

For a single harmonic mode n, the use of Eq. B4 as the exit impedance will allow numerical calculations in finite ducts to be compared to the analytical results in an infinite duct.

REFERENCES

1. E. J. Rice, "Spinning Mode Sound Propagation in Ducts with Acoustic Treatment," NASA TN D-7913, May 1975.

2. G. F. Pickett, T. G. Sofrin, and R. W. Wells, "Method of Fan Sound Mode Structure Determination," PWA-5554-3, Pratt and Whitney Aircraft, Aug. 1977. Also NASA CR-135293, 1977.

3. A. V. Saule, "Modal Structure Inferred from Static Far-Field Noise Directivity," AIAA Paper 76-574, July 1976.

4. E. J. Rice, "Multimodal Far-Field Acoustic Radiation Pattern - An Approximate Equation," AIAA Paper 77-1281, Oct. 1977.

5. B. W. Lowrie, B. J. Tester, and C. L. Morfey, "Far-Field Methods of Duct Mode Detection for Broadband Noise Sources," AIAA Paper 77-1331, Oct. 1977.

6. K. J. Baumeister, and E. C. Bittner, "Numerical Simulation of Noise Propagation in Jet Engine Ducts," NASA TN D-7339, Oct. 1973.

7. D. W. Quinn, "A Finite Difference Method for Computing Sound Propagation in Nonuniform Ducts," AIAA Paper 75-130, Jan. 1975.

8. K. J. Baumeister, "Analysis of Sound Propagation in Ducts Using the Wave Envelope Concept," NASA TN D-7719, July 1974.

9. R. K. Sigman, R. K. Majjigi, and B. T. Zinn, "Use of Finite Element Techniques in the Determination of the Acoustic Properties of Turbofan Inlets," AIAA Paper 77-18, Jan. 1977.

10. K. J. Baumeister, "Finite-Difference Theory for Sound Propagation in a Lined Duct With Uniform Flow Using the Wave Envelope Concept," NASA TP-1001, Aug. 1977.

11. A. L. Abrahamson, "A Finite Element Algorithm for Sound Propagation in Axisymmetric Ducts Containing Compressible Mean Flow," AIAA Paper 77-1301, Oct. 1977.

12. Y. Kagawa, T. Yamabuchi, and A. Mori, "Finite Element Simmulation of an Axisymmetric Acoustic Transmission System with a Sound Absorbing Wall," J. Sound Vib. 53, 357-374 (1977).

13. M. E. Goldstein, "Aeroacoustics," (McGraw Hill, New York, 1976).

14. F. B. Hildebrand, "Methods of Applied Mathematics," (Prentice-Hall, Englewood Cliffs, N. J., 1952).

15. M. Clark, and K. F. Hansen, "Numerical Methods of Reactor Analysis," (Academic Press, New York, 1964).

16. P. M. Morse, and K. U. Ingard, "Theoretical Acoustics," (McGraw Hill, New York, 1968).

17. B. R. Leonard, R. F. Schmiedlin, E. G. Stakolich, and H. E. Neumann, "Acoustic and Aerodynamic Performance of a 6-Foot-Diameter Fan for Turbofan Engines," NASA TN D-5877, July 1970.

18. F. J. Montegani, "Some Propulsion System Noise Data Handling Conventions and Computer Programs used at the Lewis Research Center," NASA TM X-3013, Mar. 1974.

19. K. Ishihara, and K. J. Bell, "Friction Factors for In-Line Square Tube Banks at Low Reynolds Number," AIChE Symp. Ser., 68, No. 118, 74-80 (1972).

20. R. Courant, and D. Hilbert, "Methods of Mathematical Physics, Volume II," (Wiley, New York, 1962).

21. W. Eversman, E. L. Cook, and R. J. Beckemeyer, "A Method of Weighted Residuals for the Investigation of Sound Transmission in Non-Uniform Ducts without Flow," J. Sound Vib. 38, 105-123 (1975).

22. R. J. Alfredson, "The Propagation of Sound in a Circular Duct of Continuously Varying Cross-Sectional Area," J. Sound Vib. 23, 433-442 (1972).

23. G. A. Korn, and T. M. Korn, "Mathematical Handbook for Scientists and Engineers," (McGraw Hill, New York, 2nd ed. 1968).

24. E. J. Rice, "Attenuation of Sound in Soft Walled Circular Ducts," Presented at the AFOSR-UTIAS Symposium on Aerodynamics Noise, Toronto, May 20-21, 1968. Also NASA TM X-52442, 1968.

25. M. N. Ozisik, "Boundary Value Problems of Heat Conduction," (International Textbook Co., London, 1968).

26. P. E. Doak, "Some Comments on Possible Back-Reaction Effects of Acoustic Fields on Aerodynamic Sound Sources," "Basic Aerodynamic Noise Research," NASA SP-207, 1969, pp. 469-472.

27. R. M. Fitzgerald, "Helmholtz Equation as an Initial Value Problem with Application to Acoustic Propagation," J. Acoust. Soc. Am. 57, 839-842 (1975).

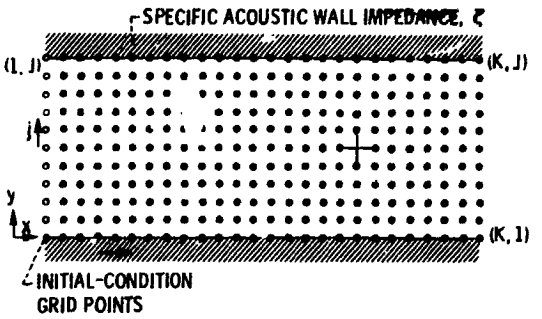

Figure 1. - Grid-point representation of two-dimensional flow duct.

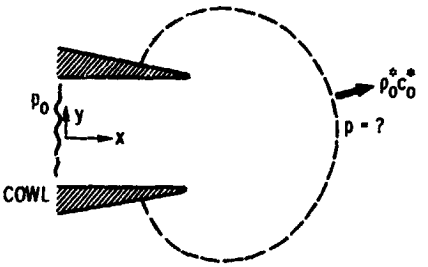

(a) BOUNDARY VALUE PROBLEM (UNKNOWN FAR FIELD PRESSURE).

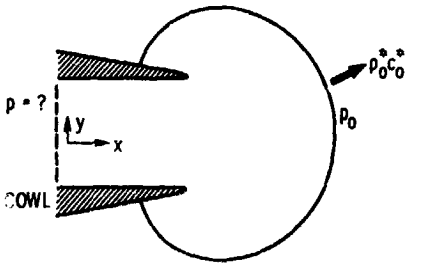

(b) FAR FIELD INITIAL VALUE PROBLEM (UNKNOWN SOURCE PRESSURE).

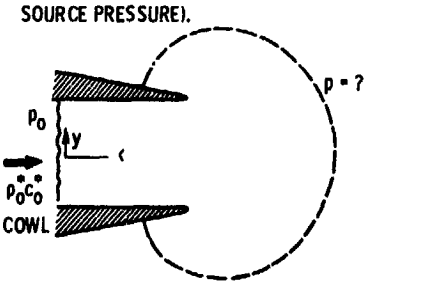

(c) SOURCE INITIAL VALUE PROBLEM (UNKNOWN FAR FIELD PRESSURE).

Figure 2. - Types of boundary and initial value problems for acoustic pressure fields.

TABLE I. - COEFFICIENTS IN EXPLICIT DIFFERENCE EQUATIONS

Cell index, m	Difference elements				
	a_m	b_m	c_m	d_m	e_m
1	$-\left(\frac{\Delta y}{\Delta x}\right)^2$	-1	$2\ 1+\left(\frac{\Delta y}{\Delta x}\right)^2-\frac{(2\pi\eta\Delta y)^2}{2}$	-1	$-\left(\frac{\Delta y}{\Delta x}\right)^2$
2	a_1	-2	$c_1+\frac{2i(2\pi\eta\Delta y)}{\zeta_w}$	0	e_1
3	a_1	0	c_2	-2	e_1
4	$2a_1$	-1	$c_1+\frac{2i(2\pi\eta)\Delta y^2}{\Delta x\zeta_e}$	-1	0
5	a_4	-2	$c_4+\frac{2i2\pi\eta\Delta y}{\zeta_w}$	0	0
6	a_4	0	c_5	-2	0
7	0	-1	$c_1-\frac{2i(2\pi\eta)\Delta y^2}{\Delta x\zeta_o}$	-1	$2e_1$
8	0	-2	$C_7\ (\zeta_w=\infty)$	0	e_7
9	0	0	$C_7\ (\zeta_w=\infty)$	-2	e_7

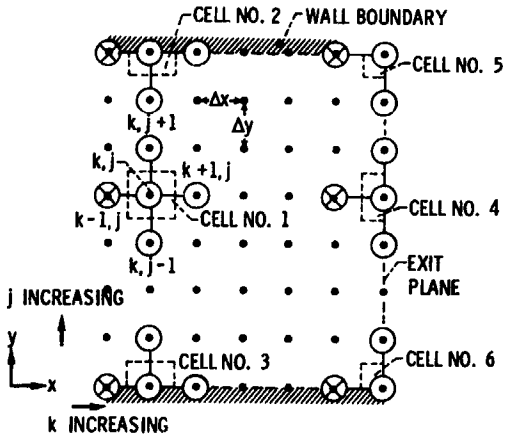

(a) BACKWARD MARCHING.

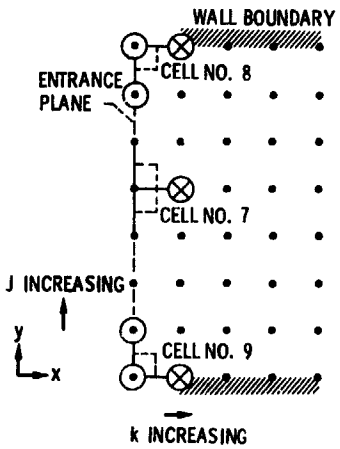

(b) FORWARD MARCHING.

Figure 3. - Coordinate and explicit grid point representation of of acoustic field.

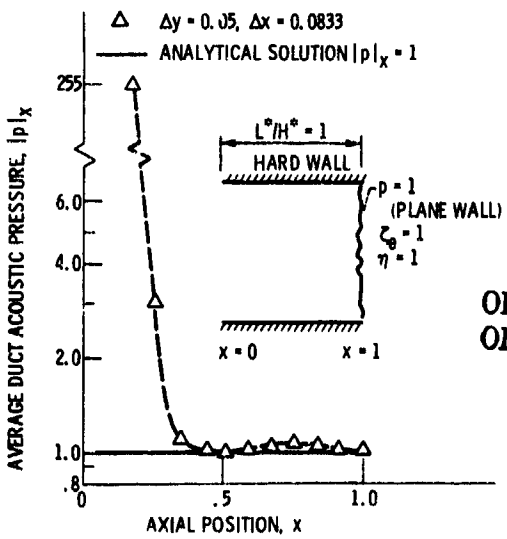

Figure 4. - Averaged integrated pressure distribution $|P|_x$ in a hard wall two dimensional duct.

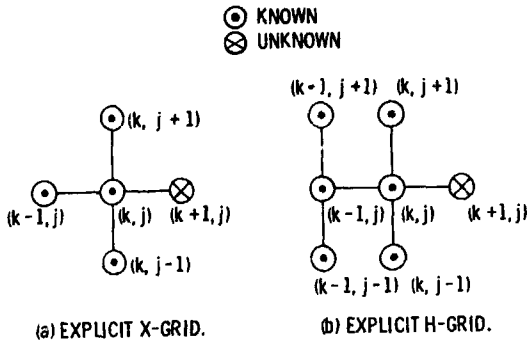

(a) EXPLICIT X-GRID. (b) EXPLICIT H-GRID.

Figure 5. - Explicit difference relationships for the Helmholtz equation.

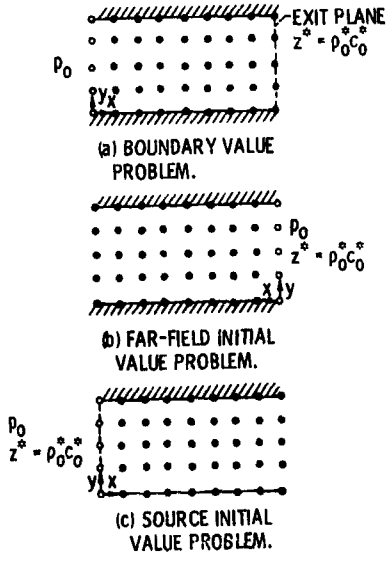

Figure 6. - Propagation problems for a ducted source.

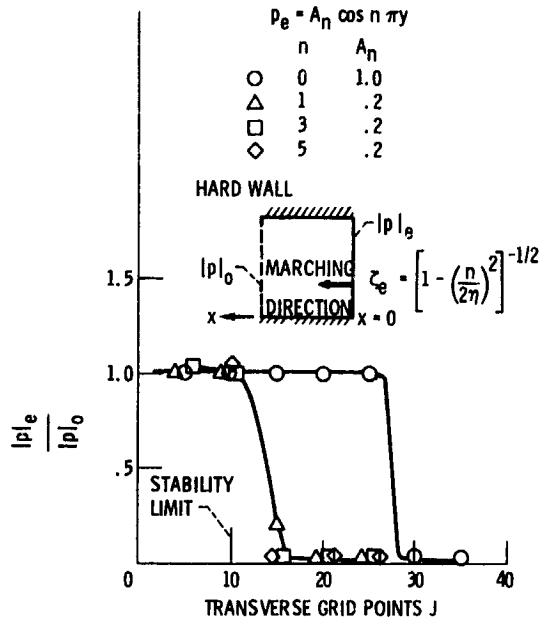

Figure 7. - Stability evaluation in marching from exit to entrance for hard wall duct (η = 3, L^*/H^* = 1, K = 36).

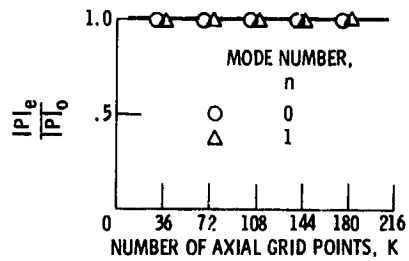

Figure 8. - Stability evaluation in marching from exit to entrance for hard wall duct (η = 3, L^*/H^* = 1, J = 10).

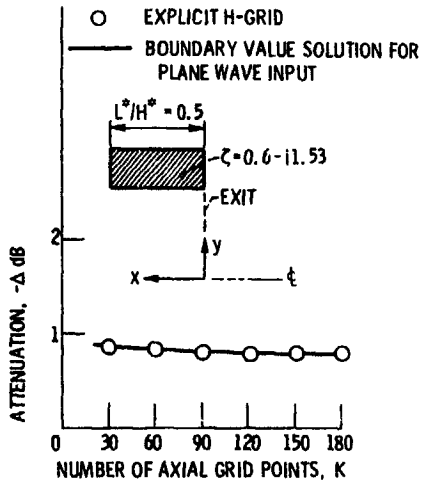

Figure 9. - Attenuation of soft wall duct as a function of axial grid spacing (η = 5, L^*/H^* = 0.5, J = 10).

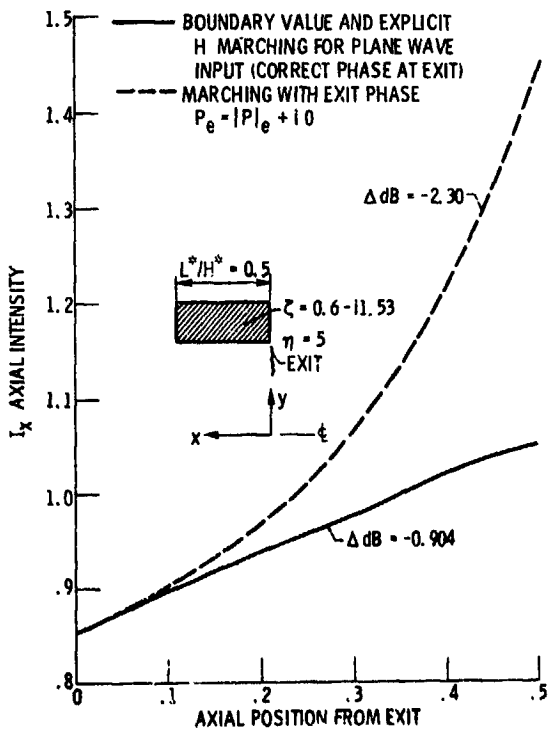

Figure 10. - Effect of exit pressure phase on acoustic intensity in a soft wall duct using explicit H marching for plane wave input at x = 0.5.

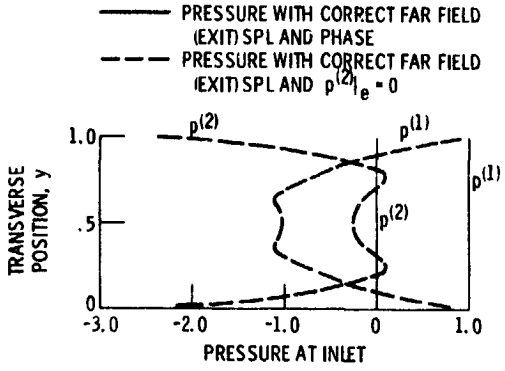

Figure 11. - Pressure profiles at duct entrance as a function of the phase at exit.

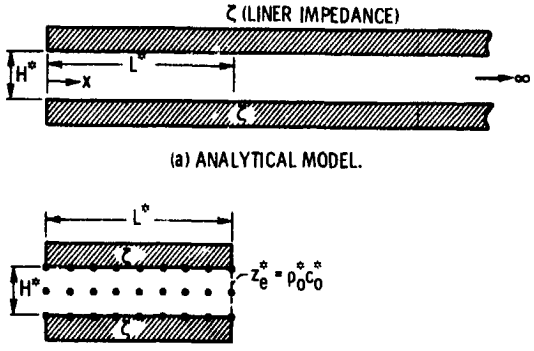

(a) ANALYTICAL MODEL.

(b) REPRESENTATION OF NUMERICAL EQUIVALENT.

Figure 12. - Numerical representation of the attenuation problem for a section L^* of an infinite duct.

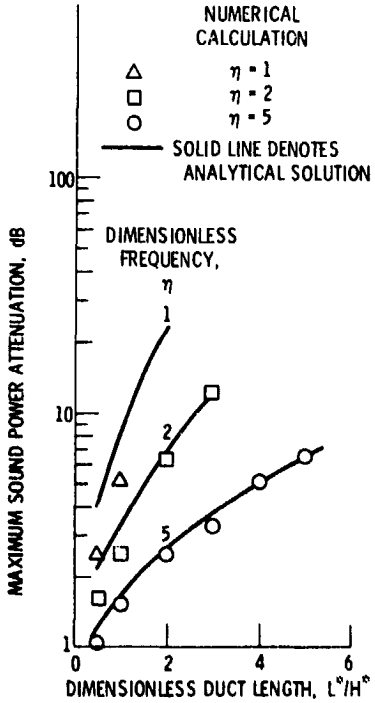

Figure 13. - Effect of axial length and frequency on attenuation at optimum impedance in two-dimensional duct for a plane wave input.